Numerical studies of the transport behavior of a passive solute in a two-dimensional incompressible random flow field

M. Dentz*
Department of Geotechnical Engineering and Geosciences, Universitat Politecnica de Catalunya, 08034 Barcelona, Spain

H. Kinzelbach
Institut für Theoretische Physik, Universität Heidelberg, Heidelberg, Germany

S. Attinger and W. Kinzelbach
Institut für Hydromechanik und Wasserwirtschaft, Eidgenössische Technische Hochschule Zürich, Zürich, Switzerland
(Received 29 October 2002; revised manuscript received 9 January 2003; published 21 April 2003)

We study the transport behavior of a passive scalar in a two-dimensional (2D) time-independent Gaussian random velocity field by efficient and highly accurate numerical simulations. The model under consideration has been used in order to gain basic understanding of transport processes in incompressible flow through heterogeneous porous media. The velocity field is derived from the linearized solution of the Darcy equation with a Gauss-distributed log-hydraulic conductivity. The transport of a passive scalar is studied by a high precision random-walk method, which allows for a systematic nonperturbative study of the ensemble and effective dispersion coefficients. The conclusive numerical results validate the range of applicability of the perturbation theory and the consistency of nonperturbative approaches to the transport problem in a random medium. Furthermore, we observe closed streamlines in incompressible 2D Gaussian random fields, which restricts the direct applicability of the simulation method for transport in heterogeneous porous media, and questions the results of similar studies that do not observe this phenomenon.

DOI: 10.1103/PhysRevE.67.046306 PACS number(s): 05.60.−k, 92.40.Kf, 47.55.Mh, 02.50.Ey

I. INTRODUCTION

The two-dimensional numerical simulations presented in this paper investigate the transport of a passive scalar in an incompressible static random velocity field. The velocity field, as an approximation to the flow field in a heterogeneous porous medium, is given by the linearized solution of the Darcy equation [1], which is a linear functional of the Gauss-distributed log-hydraulic conductivity of the medium and, as a consequence, is Gauss distributed, too. This Gaussian flow model has been used in order to study basic transport properties in heterogeneous porous media [2–7] in two and three spatial dimensions. The transport behavior of a passive scalar in similar flow models has been investigated, e.g., as a static limiting case in turbulent transport [8–11], also as an approximation for solute transport in heterogeneous porous media, and in general for the study of random walks in random environments [12–17]. In contrast to the models investigated in Refs. [8–11,14,15,17], which assume a zero mean velocity, for the modeling of transport in a heterogeneous porous medium as, e.g., a groundwater aquifer, the mean velocity is necessarily nonzero, which leads to a qualitatively and quantitatively different transport behavior [12].

As the simplest characteristic of the spatial shape of the concentration distribution, we study the temporal evolution of the macroscopic dispersion coefficients, which are defined as averages over all typical realizations of the underlying random field. We distinguish two averaging procedures which yield conceptually different dispersion quantities. The ensemble average over the dispersion coefficient in one realization of the random field defines the ''effective'' dispersion coefficient $D_{ij}^{\mathrm{eff}}(t)$, which is a measure for the spreading in one typical realization. The ''ensemble'' dispersion coefficient $D_{ij}^{\mathrm{ens}}(t)$, derived from the second centered moment of the ensemble averaged concentration distribution, in contrast, reflects the dispersion properties of the ensemble of all realizations. The conceptual difference between these two quantities has been known in the context of turbulent transport [18,19] as well as transport in time-independent random fields [20], and was investigated quantitatively in the framework of a second-order perturbation expansion in the fluctuations of the random fields in Refs. [16,21,22]. There it was found that the temporal behavior of $D_{ij}^{\mathrm{eff}}(t)$ is dominated by the dispersion time scale, $\tau_{\mathrm{D}} \equiv l^2/D$, which measures the typical time for the solute to be spread over a distance of one correlation length l of the flow field by local dispersion D. The ensemble dispersion coefficient $D_{ij}^{\mathrm{ens}}(t)$, in contrast, evolves on the advection time scale, $\tau_{\mathrm{u}} \equiv l/\overline{u}$, which represents the typical time for the solute to be transported over one correlation length of the random field by the mean drift $\overline{u}$. Both time scales are well separated in realistic situations, $\tau_{\mathrm{u}} \ll \tau_{\mathrm{D}}$ [1]. Thus, the largest times reached in the transport simulations have to be at least of the order of the (large) dispersion time scale to be able to obtain meaningful results for the effective dispersion coefficients.

The perturbative approach [13,23,24] to solve the transport problem has proved to be a valuable tool for the analytical prediction and description of macroscale transport properties in heterogeneous media. It is, however, intrinsi-

*Electronic address: marco.dentz@upc.es

cally restricted to situations of moderate heterogeneity. The efficient numerical simulations presented here are a systematic tool to investigate the relevance of higher-order contributions of the perturbation series to the transport problem for strongly fluctuating random fields. The numerical results are compared to a self-consistent resummation scheme, which in the literature is referred to as direct interaction approximation [8,10,14], Corrsin's conjecture [25–27], and fastest apparent convergence [28]. In the following we will refer to this scheme as ''Corrsin's conjecture'' (CC). In terms of a diagrammatic representation of the perturbation series, Corrsin's conjecture is a self-consistent one-loop resummation scheme, which does not account for cross diagrams. As indicated by the studies of Refs. [10,8], for the case of zero mean velocity the prediction of CC agrees very well with Monte Carlo simulations [14]. In the case of a nonzero mean drift, the situation is different. In $d=3$ spatial dimensions, the predictions of CC deviate from the results of numerical random-walk simulations [2] and describe the simulated behavior only qualitatively, which can be traced back to the systematic neglection of cross diagrams. In contrast to the second-order perturbation theory, CC predicts in $d=2$ and $d=3$ a transverse macrodispersion coefficient of ''macroscopic'' order of magnitude [i.e., it is finite in the limit of vanishing (microscopic) local dispersion] [25–27,29] as predicted by field experiments [1]. In $d=3$, this result is confirmed qualitatively by numerical simulations [2]. In $d=2$ there is strong evidence that the transverse dispersion coefficient is of the order of the (microscopic) local dispersion [29,30]. The systematic numerical simulations presented in this paper shed some new light on the range of validity of the perturbation series and the consistency of CC in $d=2$ dimensions.

For the 2D numerical studies presented in this paper we use the simulation method described in Ref. [2]. The random velocity field is generated as a superposition of a large number of randomly chosen harmonic modes [8,10,11]. The flow field generated in this way is defined continuously in every point in space. For the solution of the transport problem, we use the random-walk method as described in Ref. [8]. This method allows for efficient transport simulations combining (essential) long observation times with a large number of disorder realizations. Many numerical simulations documented in the literature, which are based on the full (numerical) or the approximate linearized solution of the Darcy equation, are limited to small observation times of only a few advection time scales and few disorder realizations [31–34], or additionally restricted to zero local dispersion, i.e., purely advective transport [6,35–37]. These studies cannot give conclusive answers to the questions posed above.

In 2D Gaussian random velocity fields one finds closed streamlines [38], a phenomenon which was observed in Ref. [10] in a Gaussian model with zero mean velocity. Closed streamlines affect the transport behavior dramatically in the case of small or zero local (microscopic) dispersion. For zero mean drift and zero local dispersion, Ref. [10] observed subdiffusion due to particle localization in closed streamlines. Here, for a finite mean drift and zero local dispersion, we observe a linear growth of the longitudinal macrodispersion coefficient. For finite local dispersion, the transport in the 2D Gaussian random field is normal in the long-time limit for the correlation function used in this study, which follows from the work of Ref. [39], see Ref. [40]. In a flow field, which solves the 2D Darcy equation for a scalar conductivity field, there cannot occur closed streamlines. Thus, the simulation method using 2D Gaussian random fields is of limited applicability to transport in heterogeneous porous media, a fact that has, to our knowledge, not been reported in the literature before. This observation questions the results of similar numerical 2D studies, which do not notice these phenomena in the limit of small or vanishing local dispersion.

II. MODEL

A. Transport

The distribution $g(\mathbf{x},t)$ of passive solute in a static incompressible random field $\mathbf{u}(\mathbf{x})$ is described by a Fokker-Planck equation:

$$\frac{\partial}{\partial t}g(\mathbf{x},t)+\overline{\mathbf{u}}\cdot\boldsymbol{\nabla}g(\mathbf{x},t)-D\Delta g(\mathbf{x},t) = \delta(\mathbf{x})\delta(t)+\mathbf{u}'(\mathbf{x})\cdot\boldsymbol{\nabla}g(\mathbf{x},t), \tag{1}$$

where we divided the stationary random field into its mean value and fluctuations about it, $\mathbf{u}(\mathbf{x})=\overline{\mathbf{u}}-\mathbf{u}'(\mathbf{x})$; the overbar denotes the ensemble average. In the following, we assume $\overline{\mathbf{u}}$ to be aligned with the one direction of the coordinate system, $\overline{u_i}=\overline{u}\delta_{i1}$. Furthermore, we assume an isotropic, constant local dispersion, which is denoted by the coefficient D. The initial condition is given by $g(\mathbf{x},t=0)=\delta(\mathbf{x})$; as boundary condition we assume a vanishing $g(\mathbf{x},t)$ at infinity.

Equation (1) can be transformed into an equivalent integral equation, which reads in Fourier space as

$$\tilde{g}(\mathbf{k},t)=\tilde{g}_0(\mathbf{k},t)-\mathrm{i}\,\mathbf{k}\cdot\int_{k'}\int_{-\infty}^{\infty}dt'\tilde{g}_0(\mathbf{k},t-t')\tilde{\mathbf{u}}'(\mathbf{k}') \times\tilde{g}(\mathbf{k}-\mathbf{k}',t-t'). \tag{2}$$

Fourier transformed quantities are denoted by a tilde, the wave vector is denoted by $\mathbf{k}$; the abbreviation $\int_{k'}\cdots \equiv\int_{\mathbb{R}^2}d^2k'/(2\pi)^2\cdots$. The unperturbed propagator is given by $\tilde{g}_0(\mathbf{k},t)=\Theta(t)\exp(-Dk^2t+i\overline{u}k_1t)$, with $\Theta(t)$ the Heaviside step function.

The effective and ensemble dispersion coefficients now can be defined in terms of $\tilde{g}(\mathbf{k},t)$:

$$D_{ij}^{\mathrm{eff}}(t)=-1/2\frac{\partial}{\partial t}\frac{\partial^2}{\partial k_i\partial k_j}\overline{\{\ln\tilde{g}(\mathbf{k},t)\}}\big|_{\mathbf{k}=\mathbf{0}}, \tag{3}$$

$$D_{ij}^{\mathrm{ens}}(t)=-1/2\frac{\partial}{\partial t}\frac{\partial^2}{\partial k_i\partial k_j}\ln\{\overline{\tilde{g}(\mathbf{k},t)}\}\big|_{\mathbf{k}=\mathbf{0}}, \tag{4}$$

respectively. The conceptual and quantitative difference between these two dispersion quantities has been discussed extensively in Refs. [21,22] in the framework of second-order

perturbation theory. By iteration of Eq. (2) one can generate a perturbation series in $\tilde{\mathbf{u}}'(\mathbf{k})$, which is the basis for their studies.

By using the translational invariance of the random field $\mathbf{u}(\mathbf{x})$, one can derive from Eq. (2) the following relation for the ensemble averaged distribution $\overline{\tilde{g}(\mathbf{k},t)}$ [40]:

$$\overline{\tilde{g}(\mathbf{k},t)} = \tilde{g}_0(\mathbf{k},t) - \int_{k'}\int_{k''}\int_{-\infty}^{\infty} dt' \int_{-\infty}^{\infty} dt'' \tilde{g}_0(\mathbf{k},t')\tilde{g}_0(\mathbf{k} - \mathbf{k}', t'-t'') \cdot k_i \{\overline{\tilde{u}_i'(\mathbf{k}')\tilde{u}_j'(\mathbf{k}'')g(\mathbf{k}-\mathbf{k}'',t'')}\} k_j, \tag{5}$$

where we sum over repeated indices. From this representation follows directly that the center of mass velocity

$$u_i^{\mathrm{eff}}(t) \equiv -i \frac{\partial}{\partial t} \frac{\partial}{\partial k_i} \overline{\tilde{g}(\mathbf{k},t)}|_{\mathbf{k}=\mathbf{0}} = \overline{u}\,\delta_{i1}.$$

The CC now assumes that in Eq. (5) for large times (i) all direct correlations between $\tilde{\mathbf{u}}'(\mathbf{k})$ and $\tilde{g}(\mathbf{k},t)$ vanish, and (ii) $\overline{\tilde{g}(\mathbf{k},t)}$ can be approximated by a Gaussian which is characterized by the center of mass velocity $\overline{u}$ and $\mathbf{D}^{\mathrm{ens}}(t)$. By using definition (4), this yields a system of self-consistent nonlinear equations [40,2,26,27] for the asymptotic long-time values of the ensemble dispersion coefficients $D_{ii}^{\infty} \equiv \lim_{t\to\infty} D_{ii}^{\mathrm{ens}}(t)$, $i=1,\ldots,d$. The off-diagonal elements of the macrodispersion tensor vanish for symmetry reasons. The results of the perturbation theory, presented in Appendix A, and CC are compared to random-walk simulations.

The Langevin equation that is associated to the Fokker-Planck equation (1) and describes the motion of one particle is given by [17,41,42]

$$\frac{d}{dt}\mathbf{x}(t) = \mathbf{u}(\mathbf{x}(t)) + \boldsymbol{\xi}(t), \tag{6}$$

where $\boldsymbol{\xi}(t)$ represents a two-dimensional Gaussian white noise defined by $\langle \xi_i(t)\rangle = 0$ and $\langle \xi_i(t)\xi_j(t')\rangle = 2D\delta_{ij}\delta(t-t')$. The angular brackets denote the average over all white noise realizations.

For advection-dominated transport situations, i.e., for large Péclet numbers $\mathrm{Pe} = \overline{u}l/D \gg 1$ (l being a typical heterogeneity length scale, which in the following is identified with the correlation length of the random field), the transport-dominating influence of the spatially heterogeneous flow field can be captured only by accurate numerical solutions of the single-particle path lines [2]. We use the extended Runge-Kutta method given in Ref. [8] (''extended'' because it accounts also for local dispersion) instead of the common Euler method which follows from a straightforward time discretization of Eq. (6). The accuracy of the extended Runge-Kutta scheme used here for the calculation of the particle path lines is of the order $\Delta t^{3/2}$ whereas the Euler method provides an accuracy of order $\Delta t^{1/2}$ only. For completeness, we give a short description of the used algorithm in Appendix A.

For the simulations, the number of realizations of the random field $\mathbf{u}(\mathbf{x})$ varies between 2000 for the investigation of the asymptotic behavior and 2500 for the temporal behavior; the number of white noise realizations varies between 100 and 150. The time discretizations were $\Delta\tau = 0.05$ and $\Delta\tau = 0.1$, where we defined the dimensionless time $\tau = t/\tau_u$.

For illustration, we express the definitions (3) and (4) of the effective and ensemble dispersion coefficients in terms of the particle position $\mathbf{x}(t)$:

$$D_{ii}^{\mathrm{eff}}(t) = 1/2 \frac{d}{dt}\{\overline{\langle x_i(t)x_i(t)\rangle} - \overline{\langle x_i(t)\rangle\langle x_i(t)\rangle}\}, \tag{7}$$

$$D_{ii}^{\mathrm{ens}}(t) = 1/2 \frac{d}{dt}\{\overline{\langle x_i(t)x_i(t)\rangle} - \overline{\langle x_i(t)\rangle}\ \overline{\langle x_i(t)\rangle}\}. \tag{8}$$

Note that the order by which the two ensemble averages are taken is relevant. The angular brackets denote the average over the white noise $\boldsymbol{\xi}(t)$, which generates the local dispersion, the overbar stands for the average over the ensemble of all possible realizations of the random flow field $\mathbf{u}(\mathbf{x})$. In the following we will employ the notation $D_L^{\mathrm{eff}}(t) = D_{11}^{\mathrm{eff}}(t)$ and $D_T^{\mathrm{eff}}(t) = D_{ii}^{\mathrm{eff}}(t)$, $i>1$, and analogously for the ensemble quantity.

B. Velocity field

Fluid flow through a heterogeneous porous medium is described by the Darcy equation [43]

$$\mathbf{u}(\mathbf{x}) = -\exp\{f(\mathbf{x})\}\boldsymbol{\nabla} h(\mathbf{x}), \tag{9}$$

where $h(\mathbf{x})$ is the hydraulic head, $f(\mathbf{x})$ the log-hydraulic conductivity, which is modeled as a translational invariant Gaussian random field; $f(\mathbf{x})$ is split into its mean value and fluctuations about it, $f(\mathbf{x}) = \overline{f} - f'(\mathbf{x})$. The linearized solution of Eq. (9) is a linear functional of f' [1]:

$$u_i(\mathbf{x}) = \overline{u}\,\delta_{i1} - \overline{u}\int_k \exp(-i\,\mathbf{k}\cdot\mathbf{x}) p_i(\mathbf{k}) \tilde{f}'(\mathbf{k}), \tag{10}$$

where the $p_i(\mathbf{k}) \equiv \delta_{1i} - k_1 k_i / k^2$ assure the incompressibility of the flow field. The autocorrelation function of the so defined velocity field reads in Fourier space as

$$\overline{\tilde{u}_i'(\mathbf{k})\tilde{u}_j'(\mathbf{k}')} = \overline{u}^2 (2\pi)^2 \delta(\mathbf{k}+\mathbf{k}') p_i(\mathbf{k}) p_j(\mathbf{k}) C_{\mathrm{ff}}(\mathbf{k}), \tag{11}$$

where we used the fact that the autocorrelation function $\overline{\tilde{f}'(\mathbf{k})\tilde{f}'(\mathbf{k}')} = C_{\mathrm{ff}}(\mathbf{k})(2\pi)^2\delta(\mathbf{k}+\mathbf{k}')$. Here, we choose for the $C_{\mathrm{ff}}(\mathbf{k})$ a Gauss-shaped function,

$$C_{\mathrm{ff}}(\mathbf{k}) = \sigma^2 (2\pi l^2) \exp\left(-\frac{k^2 l^2}{2}\right), \tag{12}$$

with the correlation length l and the variance σ^2. In the literature, one finds frequently an alternative autocorrelation model (e.g., Refs. [12,15,17,10]):

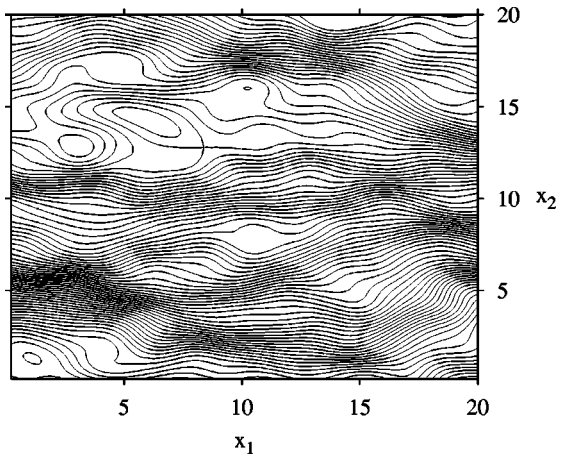

FIG. 1. Streamlines of a typical realization of the random velocity field (14) for $N=64$ random modes for $\tau_u=l/\overline{u}=1d$ and $\sigma^2=1$; x_1 and x_2 are given in units of the correlation length l.

$$\widetilde{u_i'(\mathbf{k})u_j'(\mathbf{k}')}=(2\pi)^2\delta(\mathbf{k}+\mathbf{k}')\left(\delta_{ij}-\frac{k_ik_j}{k^2}\right)C_{uu}(\mathbf{k}), \tag{13}$$

with varying $C_{uu}(\mathbf{k})$.

One realization of the Gaussian random velocity field characterized by the autocorrelation function (11) with Eq. (12) is numerically generated as a superposition of randomly chosen harmonic modes [8,10,11]:

$$u_i(\mathbf{x})=\overline{u}\delta_{i1}-\sigma\overline{u}\sqrt{\frac{2}{N}}\sum_{j=1}^{N}p_i(\mathbf{k}^{(j)})\cos(\mathbf{k}^{(j)}\cdot\mathbf{x}+\varphi^{(j)}). \tag{14}$$

The vectors $\mathbf{k}^{(j)}$ and the phases $\varphi^{(j)}$ are independent random numbers. Their distributions determine the autocorrelation function of the resulting random field $\mathbf{u}(\mathbf{x})$. The wave vectors $\mathbf{k}^{(j)}$ are drawn from a two-dimensional Gaussian distribution with vanishing average and variance $1/l^2$. The phases $\varphi^{(j)}$ are equally distributed in the interval $[0,2\pi]$. Here we used $N=64$ and convinced ourselves that a larger number of modes does not change the given results.

The so generated random flow field is Gaussian in the limit of an infinite number of random modes, $N\to\infty$. In $d=2$ spatial dimensions there is a finite probability for closed streamlines in Gaussian random flows as is derived in Appendix B and Ref. [40]. This phenomenon has already been observed by Kraichnan [10], who investigated the transport behavior for the correlation model (13) with $C_{uu}(\mathbf{k})=\sigma^2(2\pi)^{d/2}l^{2+d}k^2\exp(-k^2l^2/2)$ for $D=0$ and $\overline{\mathbf{u}}=\mathbf{0}$. He observed subdiffusive behavior for the ensemble dispersion coefficients owing to the fact that all particles were trapped within closed streamlines. Here, one observes subdiffusive behavior only for $D_T^{\mathrm{ens}}(t)$ as illustrated in Fig. 2(a). Owing to the finite drift, $\overline{u}\neq 0$, here one sees closed as well as open streamlines, which is illustrated in Fig. 1. Figure 1 shows a typical realization of the random velocity field (14) for $N=64$ random modes with $\tau_u=l/\overline{u}=1d$ and $\sigma^2=1$. Thus, particles can be trapped within closed streamlines and advected freely along open streamlines. This topological property leads to a linear growth of the longitudinal dispersion coefficient with time, which is illustrated in Fig. 2(b). A phenomenological model that explains this linear growth on the basis of the existence of closed streamlines is presented in Appendix C. Until now this behavior has not been observed in similar transport simulations, most probably due to numerical integration error, which mimics a local dispersion. These trapping phenomena are observed in every truly Gaussian flow field, as is shown in Appendix B. Thus, the results of numerical studies using Eq. (10), which do not observe these trapping phenomena in the limiting case $D=0$, are questionable.

For $D\neq 0$, the transport behavior is normal in the long-time limit [39] and $D_L^{\mathrm{ens}}(t)$ converges to a finite constant because the local dispersion causes an exchange of particles between closed and open streamlines

In passing, let us also comment on another subtle point related to the way the Gaussian random flow field is generated. The velocity field given by Eq. (14) as a superposition of N randomly chosen harmonic modes is Gaussian only in the limit $N\to\infty$. For a finite number of random modes, $N<\infty$, the number of closed streamlines vanishes for a certain (small) variance σ^2. However, this numerical artifact disappears in the limit of $N\to\infty$.

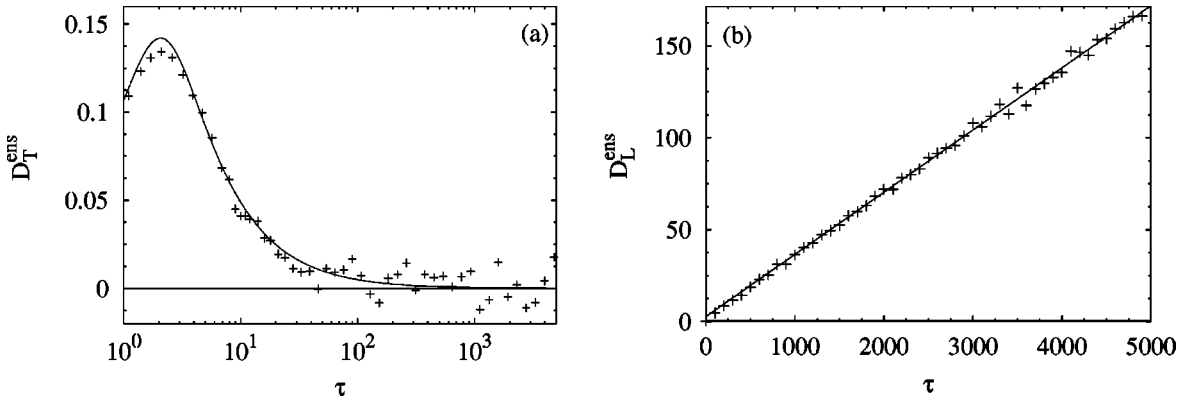

FIG. 2. Simulated behavior of (a) D_T^{ens} and (b) D_L^{ens} versus nondimensional time $\tau=t/\tau_u$ for $\mathrm{Pe}=\infty$, $\sigma^2=1$. The data points are given by (+), the solid line in (a) shows the second-order perturbation theory, the solid line in (b) denotes a linear fit to the data.

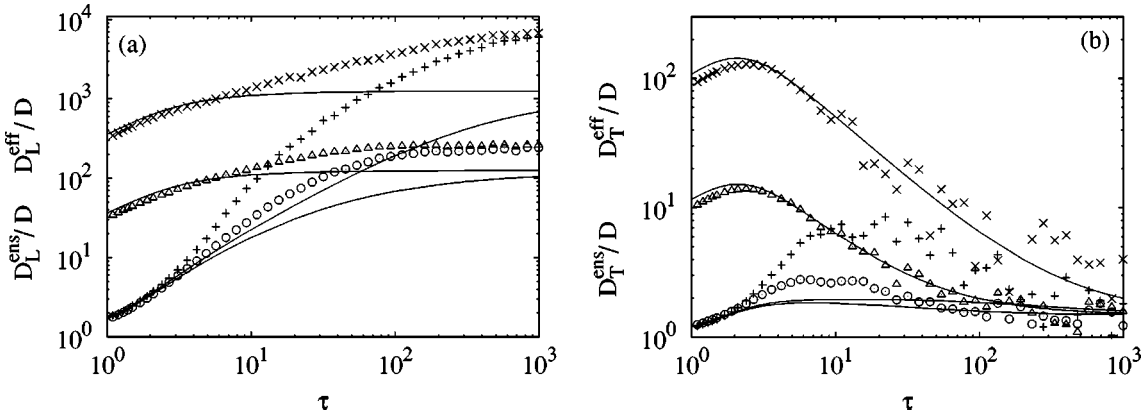

FIG. 3. Simulated temporal behavior for (a) D_L^{eff} and D_L^{ens} and (b) D_T^{eff} and D_T^{ens} for $\sigma^2=1$; $(\times)$ and $(+)$ denote the respective data for $\mathrm{Pe}=10^3$, $(\odot)$ and $(\triangle)$ for $\mathrm{Pe}=10^2$. The solid lines are the corresponding expressions from second-order perturbation theory.

For the full solution of the Darcy equation there exist no closed streamlines as is shown in Appendix D. This observation indicates a limitation of the applicability of the flow model (10) to transport in 2D heterogeneous porous media and makes it inapplicable in the case $D=0$. Nevertheless, the use of a Gaussian random velocity provides basic insight into analytical and semianalytical methods to solve for transport in a spatially varying velocity field. Note, for example, that the behavior of D_T^{ens} illustrated in Fig. 2(a) contradicts CC, which predicts in $d=2$ and $d=3$ a finite value for the asymptotic transverse dispersion. The simulations confirm the perturbation theory [29] and an exact result [30] obtained in the limit $D=0$. Furthermore, it is interesting to note that second-order perturbation theory describes the simulation data surprisingly well for a relatively ''high'' variance σ^2.

III. RESULTS

The stochastic approach is meaningful only for times large compared to the advection time scale τ_{u} [2]. Thus, we focus on transport times $t \geqslant \tau_{\mathrm{u}}$. The time in the following is measured in units of the advection time scale, $\tau = t/\tau_u$. Thus, in terms of the nondimensional time τ, the intermediate time regime is given by $1 \ll \tau \ll \mathrm{Pe}$, the long-time regime by $\tau \gg \mathrm{Pe}$ because $\mathrm{Pe} = \tau_D/\tau_u$. For small variances the simulation results, which are not shown here, confirm the temporal behavior predicted by the second-order perturbation theory for the longitudinal and transverse dispersion coefficients.

Figures 3(a) and 3(b) illustrate the simulated temporal behavior of the longitudinal and transverse effective and ensemble dispersion coefficients for $\sigma^2=1$ and $\mathrm{Pe}=10^2$ and $\mathrm{Pe}=10^3$ compared to the corresponding second-order perturbation theory results, see Appendix A. The simulated temporal behavior of D_L^{eff} and D_L^{ens}, Fig. 3(a), is quantitatively different from the behavior predicted by the perturbation theory, which underestimates the observed values. In the intermediate time regime $1 \ll \tau \ll \mathrm{Pe}$, one observes an unexpected strong growth of D_L^{eff} and D_L^{ens}. The effective and ensemble quantities converge to a constant asymptotic value on the dispersion time scale τ_D, which is described qualitatively by the perturbation theory. The D_L^{ens}, however, reaches its asymptotic long-time value much later than the corresponding second-order expressions. The observed temporal evolution of the observables can be explained by the influence of the complicated streamline structure, which is more important for large Péclet numbers, i.e., advection-dominated transport situations. The unexpected strong increase of the dispersion coefficients in the intermediate time regime can be traced back to trapping phenomena related to the closed streamlines within the Gaussian velocity field (14). These phenomena are not accounted for by lowest-order perturbation theory. Closed streamlines define stagnation zones, where particles may be trapped, in contrast to regions of fast particle transport along open streamlines. Local dispersion provides an exchange mechanism for particles between these immobile zones and mobile regions of fast transport. The smaller the local dispersion coefficient, i.e., the larger the Peclet number, the larger is the mean trapping time for the particles. This effect obviously enhances the longitudinal dispersion, and leads to the strong increase of D_L^{eff} and D_L^{ens} observed in Fig. 3(a).

In Fig. 3(b), we see the time behavior of the transverse dispersion coefficients. The D_T^{ens} agree well with the second-order expressions for $\mathrm{Pe}=10^2$ and $\mathrm{Pe}=10^3$. The D_T^{eff} in contrast is underestimated by the perturbation theory in the intermediate time regime, $1 \ll \tau \ll \mathrm{Pe}$. For long times, D_T^{eff} and D_T^{ens} converge to the same asymptotic value, which is of the order of the local dispersion coefficient in contrast to $d=3$, for which a macroscopic disorder-induced contribution was found [2]. The simulated long-time behavior confirms the second-order perturbation theory, which predicts that there is no macroscopic contribution to the asymptotic long-time value of the transverse dispersion coefficient. It is a remarkable fact that the temporal behavior of the ensemble dispersion coefficient is well described by the second-order perturbation theory expression even for a relatively large σ^2.

Figures 4 and 5 show the simulated behavior of the asymptotic longitudinal and transverse dispersion coefficients versus σ^2 and versus Pe^{-1}, respectively. In the following, the asymptotic values will be denoted by $D_L^{\infty} = \lim_{t\to\infty} D_L^{\mathrm{eff}}(t)$ and for the transverse coefficient accord-

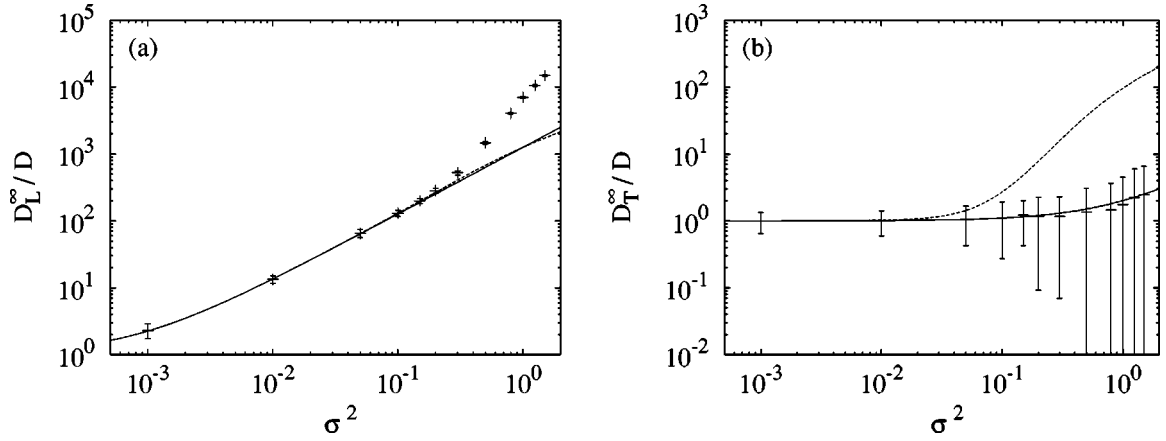

FIG. 4. Simulation data for (a) D_L^∞, (b) D_T^∞ versus σ^2 for $\mathrm{Pe}=10^3$. The dashed line illustrates CC, the solid line second-order perturbation theory.

ingly. The asymptotic dispersion coefficients are calculated as time averages of D_L^{ens} and D_T^{ens} over an interval where they already reached their final values. The error bars given in the results below are defined as the root mean squared deviations from these averages. The simulation results are compared to the corresponding results from CC and second-order perturbation theory.

Figures 4(a) and 4(b) show the behavior of the D_L^∞ and D_T^∞ versus σ^2 for $\mathrm{Pe}=10^3$. For small σ^2 the second-order results and the almost identical results from CC agree well with the simulation data. For increasing σ^2, both analytical approaches underestimate the simulated D_L^∞, Fig. 4(a), remarkably. Note that for the σ^2 values under consideration, CC is almost indistinguishable from the second-order prediction.

For the transverse dispersion coefficients, shown in Fig. 4(b), one observes a significant discrepancy between the simulation data and CC for large σ^2. CC predicts a transverse dispersion coefficient of macroscopic order of magnitude. The simulated D_T^∞, however, agree well with the second-order expressions, which are of the order of magnitude of the local dispersion coefficient, i.e., small. The erroneous behavior predicted by CC can be traced back to the fact that essential higher-order contributions to the asymptotic dispersion coefficients are neglected [30,29,40,27].

Figures 5(a) and 5(b) illustrate the dependence of D_L^∞ and D_T^∞ on Pe^{-1} for $\sigma^2=1$. For small Pe, the transport is diffusion dominated and D_L^∞ and D_T^∞ increase with decreasing Pe, i.e., increasing D. For increasing Pe, D_L^∞, Fig. 5(a), decreases and assumes a minimum. Then it increases for $\mathrm{Pe}\to\infty$. This behavior for D_L^∞ reflects the behavior, which we observed for $D_L^{\mathrm{ens}}(t)$ in the limiting case $D=0$ ($\mathrm{Pe}=\infty$), see Fig. 2(b). Second-order perturbation theory and CC underestimate the simulation data considerably for large Péclet numbers, which again indicates the importance of higher-order contributions. The D_T^∞, Fig. 5(b), decreases monotonically for increasing Pe, also reflecting the behavior observed in the temporal behavior of $D_T^{\mathrm{ens}}(t)$ for $D=0$ in Fig. 2(a). The simulation data are described well by second-order perturbation theory and considerably overestimated by CC.

The simulation results show the influence of the streamline structure for advection-dominated transport, i.e., high Peclet numbers. The results for the transverse dispersion coefficients indicate that CC is inconsistent as a resummation scheme for the perturbation series and yields erroneous results for high Péclet numbers.

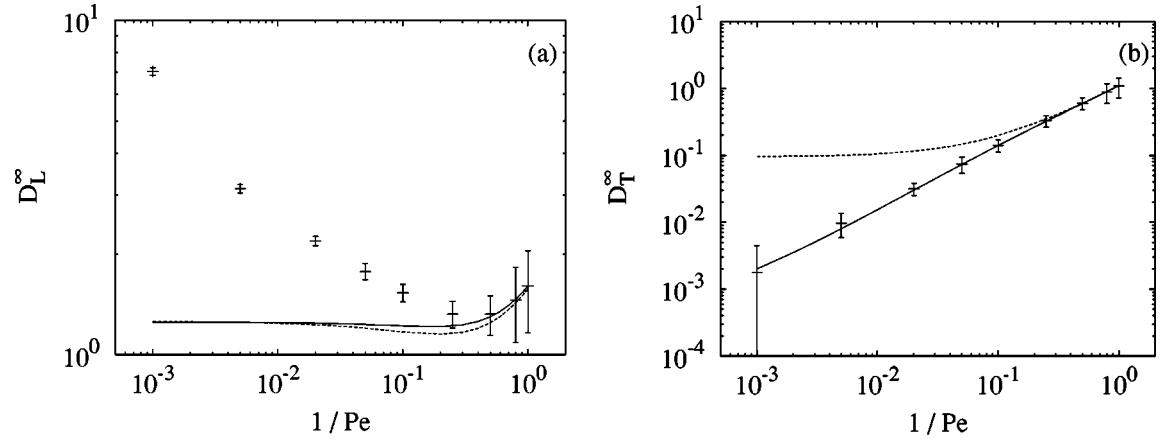

FIG. 5. Simulation data for (a) D_L^∞, (b) D_T^∞ versus 1/Pe for $\sigma^2=1$. The dashed line illustrates CC, the solid line second-order perturbation theory.

IV. SUMMARY

We investigated the transport behavior of a passive scalar in a 2D spatially varying velocity field which is given by the linearized solution of the Darcy equation. The log-hydraulic conductivity $f(\mathbf{x})$ is modeled as a Gaussian random field. Consequently, the velocity $\mathbf{u}(\mathbf{x})$, being a linear functional of $f(\mathbf{x})$, is a 2D Gaussian random field. The statistical properties of this $\mathbf{u}(\mathbf{x})$ are well defined and the statistical topography is well known [10,38], in contrast to the full solution of the Darcy equation. We showed analytically that in any incompressible Gaussian random field there is a finite probability for closed streamlines, and investigated numerically the influence on the transport behavior. In the extreme case of zero local dispersion, the longitudinal spreading is characterized by a longitudinal ensemble dispersion coefficient which grows linearly with time. These phenomena should be observed in every numerical study that uses the linearized solution of the Darcy flow field for a log-normal hydraulic conductivity. If this is not the case, these phenomena are lost due to numerical inaccuracies and the simulation parameters are not well defined. The results obtained by such simulations are at least questionable. This investigation of transport in such a flow field stresses the importance of an accurate numerical description of the streamlines in order to capture the influence on the transport behavior in advection-dominated transport situations appropriately.

In contrast to the linearized solution, the full solution of the Darcy equation does not have closed streamlines. Thus, the applicability of the simulation method using a Gaussian-distributed velocity field to approximate the flow in two-dimensional heterogeneous porous media is limited. However, most analytical methods to solve the transport problem use Gaussian random fields. Thus, despite the fact that the used velocity fields need not be realistic for flow in heterogeneous porous media, they allow for a consistent check of the validity of the perturbation theory and Corrsin's conjecture. The numerical model used in this study provides nonperturbative solutions to the transport problem combining long observation times with a large number of disorder realizations and is therefore suited to validate the consistency of these approaches.

The numerical results presented here differ from those of other authors not only by the high degree of accuracy by which the streamlines have been calculated but also by the times up to which the evolution of the transport parameters is followed in terms of the characteristic dispersion and advection time scales. It was possible to study systematically the temporal behavior of the ensemble and effective dispersion coefficients in $d=2$ spatial dimensions. For small values of σ^2 the simulation data and the expressions derived from perturbation theory were in good agreement whereas for increasing σ^2 we found systematic deviations from the perturbative behavior. Yet, the simulated behavior confirms the quantitative difference between the ensemble and effective quantity for finite times predicted by second-order perturbation theory. Furthermore, we investigated the asymptotic longitudinal and transverse macroscale dispersion coefficients as a function of σ^2 and the local dispersion coefficient D. We found that the perturbation theory and Corrsin's conjecture describe the simulation results adequately for small values of σ^2 and for large values of D. When the fluctuations of the random velocity field increase, however, one observes significant deviations from the behavior predicted by the analytical approaches. The longitudinal dispersion coefficient is underestimated by both approaches. The transverse dispersion coefficient found in the simulations turned out to be of the order of the local dispersion coefficient (i.e., negligibly small) in agreement with the second-order perturbation theory. This result is completely contrary to Corrsin's conjecture, which predicts a macroscopic asymptotic value and indicates the inconsistency of Corrsin's conjecture for transport in static incompressible random field.

The investigation of transport in a well defined random velocity field sheds some new light on the stochastic modeling approach to transport in heterogeneous flow fields. The presented numerical study allowed for a conclusive comparison of the exact numerical solutions and results from analytical solution methods to the transport problem, which gave important insights into their applicability and limitations.

APPENDIX A: EXPLICIT INTEGRAL EXPRESSIONS FOR THE MACRODISPERSION COEFFICIENTS IN $d=2$ SPATIAL DIMENSIONS

We develop explicit integral expressions for the ensemble and effective dispersion coefficients by evaluating the d-dimensional formulas given in Ref. [22] for $d=2$. For an isotropic velocity spectrum $l_1=l_2=\cdots=l_d\equiv l$, and an isotropic and constant local dispersion tensor, $D_L=D_T\equiv D$, the effective and ensemble dispersion coefficients are given by

$$D_{ii}^{\mathrm{ens}}(t)=D+\overline{ul}M_i^-(t/\tau_{\mathrm{u}},0), \tag{A1}$$

$$D_{ii}^{\mathrm{eff}}(t)=D_{ii}^{\mathrm{ens}}(t)-\overline{ul}M_i^+(t/\tau_{\mathrm{u}},2t/\tau_{\mathrm{D}}), \tag{A2}$$

where the $M_i^{\pm}(T,b)$ are given by

$$M_1^{\pm}(T,b)=\frac{3}{8}(1+2b)^{-1/2}\int_0^{T\lambda/(2\epsilon)}dx\left\{8\frac{(1\pm\lambda x)}{x^4}\times\left[\exp\left(\frac{-x^2}{2(1\pm\lambda x)}\right)-1\right]+\frac{4}{x^2}\right\}, \tag{A3}$$

$$M_2^{\pm}(T,b)=(1+2b)^{-1/2}\int_0^{T\lambda/(2\epsilon)}dx\left[\frac{-1}{2x^2}+3\frac{(1\pm\lambda x)}{x^4}-\exp\left(\frac{-x^2}{2(1\pm\lambda x)}\right)\left(3\frac{(1\pm\lambda x)}{x^4}+\frac{1}{x^2}\right)\right], \tag{A4}$$

with

$$\lambda=2\epsilon(1+2\,b)^{-1/2},\quad \epsilon=\mathrm{Pe}^{-1}. \tag{A5}$$

The resulting integral expressions involve only one integration, which can be easily performed numerically.

APPENDIX B: EXTENDED RUNGE-KUTTA METHOD ACCORDING TO DRUMMOND *et al.* [8]

In order to solve the equation of motion of a solute particle in one realization of $\mathbf{u}(\mathbf{x})$ subject to a Gaussian white noise, we use an extended Runge-Kutta scheme. According to Drummond *et al.* [8], an Nth-order extended Runge-Kutta scheme is obtained by introducing a sequence of N points $(\mathbf{x}^{(0)},\ldots,\mathbf{x}^{(N)})$, where $\mathbf{x}^{(0)}=\mathbf{x}$ and $\mathbf{x}^{(N)}=\mathbf{x}+\Delta\mathbf{x}$. The intermediate points then are given by

$$\mathbf{x}^{(i)}=\mathbf{x}^{(0)}+\sum_{j=1}^{i}(\alpha_{ij}\boldsymbol{\mu}^{(j)}+\beta_{ij}\boldsymbol{\epsilon}^{(j)}), \tag{B1}$$

$$\boldsymbol{\mu}^{(i)}=\mathbf{u}(\mathbf{x}^{(i-1)})\Delta t, \tag{B2}$$

$$\boldsymbol{\epsilon}^{(i)}=(2D_{ii}\Delta t)^{1/2}\boldsymbol{\eta}^{(i)}, \tag{B3}$$

where $i=1,\ldots,N$, and $\boldsymbol{\eta}^{(i)}$ are a set of independent Gaussian random variables with unit variance and zero mean. The optimal choice of the coefficients α_{ij} and β_{ij} is such as to increase the accuracy of the path $\mathbf{x}(t)$ to $O(\Delta t^{(N+1)/2})$. This is exactly possible only in the case $N=2$. We use the extended Runge-Kutta scheme of order $N=3$ given in Ref. [8]. In this case there is a set of coefficients that minimizes the error at $O(\Delta t^{3/2})$:

$$\beta_{31}=\beta_{21}=\beta_{11},\quad \beta_{32}=\beta_{22} \tag{B4}$$

and

j	1	2	3
α_{3j}	0.249 975 09	0.370 791 31	0.379 233 54
β_{3j}	0.814 100 00	−0.087 663 69	0.574 069 91
α_{2j}	0.007 332 32	0.663 111 91	
α_{1j}	0.662 758 81		

(B5)

APPENDIX C: EXISTENCE OF CLOSED STREAMLINES IN 2D GAUSSIAN RANDOM FIELDS

An incompressible flow field in two dimensions can be represented by a stream function $\psi(\mathbf{x})$:

$$\mathbf{u}(\mathbf{x})=\begin{pmatrix}\partial_2\psi(\mathbf{x})\\ -\partial_1\psi(\mathbf{x})\end{pmatrix}. \tag{C1}$$

The streamlines of $\mathbf{u}(\mathbf{x})$ are given by the isolines of $\psi(\mathbf{x})$ (e.g., Ref. [43]). In the vicinity of extrema of $\psi(\mathbf{x})$ the streamlines of $\mathbf{u}(\mathbf{x})$ are closed, whereas in the neighborhood of saddle points of $\psi(\mathbf{x})$ the streamlines are hyperbolic. In the following we show that there is a nonvanishing probability for extreme points of the stream function $\psi(\mathbf{x})$ for a Gaussian random flow field.

The starting point of this analysis is the following identity [44]:

$$\int d^2x\,\delta\{\mathbf{u}(\mathbf{x})\}f(\mathbf{x})=\sum_n |J(\mathbf{x}_n)|^{-1}f(\mathbf{x}_n), \tag{C2}$$

where $\delta\{\mathbf{u}(\mathbf{x})\}$ is the two-dimensional Dirac δ distribution and $f(\mathbf{x})$ is an arbitrary function. The $\mathbf{x}_n$ are zeros of $\mathbf{u}(\mathbf{x})$, which correspond to extrema and saddle points of the stream function $\psi(\mathbf{x})$. The Jacobi matrix of $\mathbf{u}(\mathbf{x})$ is defined by

$$J_{ij}(\mathbf{x})\equiv\frac{\partial u_j(\mathbf{x})}{\partial x_i}, \tag{C3}$$

and $J(\mathbf{x})\equiv\det\mathbf{J}(\mathbf{x}_n)$ is the Jacobi determinant. For the choice $f(\mathbf{x})\equiv|J(\mathbf{x})|$, expression (C2) counts the number of extrema of $\psi(\mathbf{x})$:

$$N_{\mathrm{ex}}=\int d^2x\,\delta\{\mathbf{u}(\mathbf{x})\}|J(\mathbf{x})|\Theta\{J(\mathbf{x})\}, \tag{C4}$$

where $\Theta\{J(\mathbf{x})\}$ denotes the Heaviside step function, which assures that only extrema of $\psi(\mathbf{x})$ are counted. The sufficient condition for extrema of $\psi(\mathbf{x})$ is the definiteness of the Hesse matrix, which corresponds to $J(\mathbf{x})>0$. The integrand in Eq. (B4) is the average number of extrema per unit area:

$$\overline{n}_{\mathrm{ex}}=\delta\{\mathbf{u}(\mathbf{x})\}|J(\mathbf{x})|\Theta\{J(\mathbf{x})\}. \tag{C5}$$

The components of the flow field $u_i(\mathbf{x})$ and its derivatives $\partial u_j(\mathbf{x})/\partial x_i$ are uncorrelated, which can be verified using the incompressibility condition $\boldsymbol{\nabla}\cdot\mathbf{u}(\mathbf{x})=0$. Thus, $\mathbf{u}(\mathbf{x})$ and $J(\mathbf{x})$ are uncorrelated. Correspondingly, Eq. (B5) can be rewritten according to

$$\overline{n}_{\mathrm{ex}}=\overline{\delta\{\mathbf{u}(\mathbf{x})\}}\quad\overline{|J(\mathbf{x})|\Theta\{J(\mathbf{x})\}}. \tag{C6}$$

Since we consider Gaussian random fields, $\overline{\delta(\mathbf{u}(\mathbf{x}))}$ can be evaluated explicitly as it involves only Gauss integrations. One obtains

$$\overline{\delta\{\mathbf{u}(\mathbf{x})\}}=\frac{2\pi}{\det\mathbf{C}(0)}\exp\{-2\overline{u^2}C_{11}^{-1}(0)\}, \tag{C7}$$

where the elements $C_{ij}(\mathbf{x})$ of the autocorrelation matrix of $\mathbf{u}(\mathbf{x})$ are defined by Eq. (11); $C_{11}^{-1}(\mathbf{x})$ denotes the 11-coefficient of the inverse correlation matrix. The expression $A\equiv\overline{\Theta(J(\mathbf{x}))|J(\mathbf{x})|}$ is nonzero for the following reasons: The Jacobi determinant $J(\mathbf{x})$ vanishes identically only in the trivial case $\mathbf{u}(\mathbf{x})=\mathrm{const}$, as a consequence of the incompressibility condition $\boldsymbol{\nabla}\cdot\mathbf{u}(\mathbf{x})=0$. Furthermore, if $J(\mathbf{x})<0$ for all $\mathbf{x}$, then A would vanish because of $\Theta\{J(\mathbf{x})\}$ and the zeros of $\mathbf{u}(\mathbf{x})$ would correspond to saddle points of $\psi(\mathbf{x})$. In this case there would be only saddle points and no extrema. It can be shown, however, that the number of saddle points and the number of extrema here are equal. Thus, we conclude that A is nonzero. The average density of extrema of $\psi(\mathbf{x})$ then is given by

$$\overline{n}_{\mathrm{ex}}=\frac{2\pi A}{\det\mathbf{C}(0)}\exp\{-2\overline{u^2}C_{11}^{-1}(0)\}>0. \tag{C8}$$

The probability density for maxima and minima of the stream function of a Gaussian flow field and correspondingly for closed streamlines is finite.

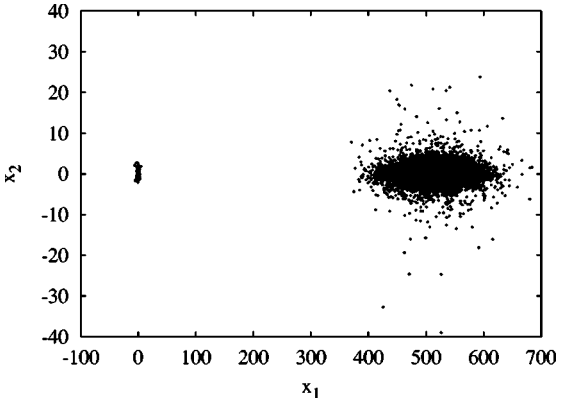

FIG. 6. Distribution of 10 000 particles at time $\tau=500$, which have been released at $\mathbf{x}=\mathbf{0}$. The random velocity field is characterized by $\tau_u=1\ d$ and $\sigma^2=1$; x_1 and x_2 are measured in units of the correlation lengths l.

APPENDIX D: LINEAR GROWTH OF THE LONGITUDINAL DISPERSION COEFFICIENT FOR AN INFINITE PECLET NUMBER

Figure 6 illustrates the average distribution of 10 000 particles at $\tau=500$ for $\mathrm{Pe}=\infty$, transported in the random velocity field (14) for $N=64$ modes $\tau_u=1\ d$ and $\sigma^2=1$. The particle distribution separates into a mobile part and a localized part centered about the injection point at $\mathbf{x}=\mathbf{0}$.

The long-time behavior of the longitudinal ensemble dispersion coefficient of such a (average) distribution, as illustrated in Fig. 2(b), can be derived by considering the following phenomenological model motivated by the particle distribution shown in Fig. 6. For $\tau\gg 1$, the ensemble averaged distribution can be approximated by

$$g(\mathbf{x},t)=\rho f_{\mathrm{loc}}(\mathbf{x})+(1-\rho)f_{\mathrm{mob}}(\mathbf{x},t), \tag{D1}$$

where $f_{\mathrm{loc}}(\mathbf{x},t)$ represents the localized and $f_{\mathrm{mob}}(\mathbf{x},t)$ the mobile concentration. We normalize $f_{\mathrm{loc}}(\mathbf{x})$ and $f_{\mathrm{mob}}(\mathbf{x},t)$ according to $\int d^2x\, f_{\mathrm{loc}}(\mathbf{x})=\int d^2x\, f_{\mathrm{mob}}(\mathbf{x},t)=1$. The coefficient ρ then denotes the fraction of the localized particles and correspondingly $1-\rho$ the fraction of the mobile ones. Motivated by Fig. 6, we make the following assumptions for the first and second moments of the localized distribution: The first moment in direction of $\overline{\mathbf{u}}$ of the localized part of the concentration distribution is zero, since the particles which are injected into a closed streamline at $\mathbf{x}=\mathbf{0}$ remain trapped in the vicinity of this point. The second moment of the localized distribution in direction of the mean velocity is constant and given by the typical diameter of the closed streamlines. This means

$$\begin{aligned}\int d^2x x_1 f_{\mathrm{loc}}(\mathbf{x})&=m^{(1)}_{\mathrm{loc}}=0,\\ \int d^2x x_1^2 f_{\mathrm{loc}}(\mathbf{x})&=m^{(2)}_{\mathrm{loc}}=\mathrm{const.}\end{aligned} \tag{D2}$$

Furthermore, we assume that for $\tau\gg 1$, the mobile concentration distribution can be characterized by the center of mass velocity u^* which is aligned with the one direction of the coordinate system and a diagonal (macroscopic) dispersion tensor $\mathbf{D}^*$. Thus, we obtain the following for the first and second moments of the mobile concentration distribution in one direction:

$$\begin{aligned}\int d^2x x_1 f_{\mathrm{mob}}(\mathbf{x})&=m^{(1)}_{\mathrm{mob}}=u^*t,\\ \int d^2x x_1^2 f_{\mathrm{mob}}(\mathbf{x})&=m^{(2)}_{\mathrm{mob}}=(u^*t)^2+2D_L^*t,\end{aligned} \tag{D3}$$

where D_L^* denotes the longitudinal (macroscopic) dispersion coefficient of the mobile concentration distribution. With these assumptions, one derives the following for the apparent longitudinal dispersion coefficient of the total concentration distribution $g(\mathbf{x},t)$:

$$\begin{aligned}D_L^{\mathrm{ens}}(t)&=\frac{1}{2}\frac{d}{dt}\left\{\int d^2x x_1^2 g(\mathbf{x},t)-\left(\int d^2x x_1 g(\mathbf{x},t)\right)^2\right\}\\ &=\rho D_L^*+\rho(1-\rho)u^{*2}t,\end{aligned} \tag{D4}$$

which describes the linear growth of the longitudinal ensemble dispersion coefficient observed in Fig. 2(b).

APPENDIX E: STREAMLINES IN 2D DARCY FLOW FIELDS

Here, we show that the full solution of the Darcy equation for a scalar hydraulic conductivity field in $d=2$ dimensions cannot have closed streamlines. Since in a Gaussian random field there is a finite probability for closed streamlines, it has to be concluded that the distribution of random Darcy flow fields cannot be Gaussian in $d=2$ dimensions.

We consider the properties of the stream function $\psi(\mathbf{x})$ for Darcy flow in the vicinity of zeros of $\mathbf{u}(\mathbf{x})$. From the Darcy equation one derives the following for the stream function $\psi(\mathbf{x})$:

$$\Delta\psi(\mathbf{x})+\nabla\psi(\mathbf{x})\cdot\nabla f(\mathbf{x})=0. \tag{E1}$$

The condition $\nabla\psi(\mathbf{x})=0$ for extrema or saddle points of $\mathbf{u}(\mathbf{x})$ implies $\Delta\psi(\mathbf{x})=0$. For extrema of $\psi(\mathbf{x})$ the Hesse matrix is positive or negative definite. However, since $\Delta\psi(\mathbf{x})=0$, the eigenvalues $\lambda_i, i=1,2$, of the Hesse matrix of $\psi(\mathbf{x})$ are given by

$$\lambda_{1/2}=\pm\sqrt{\left(\frac{\partial^2\psi(\mathbf{x})}{\partial x_1^2}\right)^2+\left(\frac{\partial^2\psi(\mathbf{x})}{\partial x_1\partial x_2}\right)^2}. \tag{E2}$$

Thus, the Hesse matrix is indefinite and consequently there are no maxima or minima for the stream function $\psi(\mathbf{x})$ and accordingly no closed streamlines.

[1] L.W. Gelhar and C.L. Axness, Water Resour. Res. **19**, 161 (1983).
[2] M. Dentz, H. Kinzelbach, S. Attinger, and W. Kinzelbach, Water Resour. Res. **38**, 23-1 (2002).
[3] U. Jaeckel and H. Vereecken, Water Resour. Res. **33**, 2287 (1997).
[4] V. Kapoor and P.K. Kitanidis, Transp. Porous Media **21**, 91 (1996).
[5] D. McLaughlin and F. Ruan, Transp. Porous Media **42**, 133 (2001).
[6] Y. Rubin, Water Resour. Res. **26**, 133 (1990).
[7] H. Schwarze, U. Jaeckel, and H. Vereecken, Transp. Porous Media **43**, 245 (2001).
[8] I.T. Drummond, S. Duane, and R.R. Horgan, J. Fluid Mech. **138**, 75 (1984).
[9] T. Komorowski and S. Olla, J. Stat. Phys. **108**, 647 (2002).
[10] R.H. Kraichnan, Phys. Fluids **13**, 22 (1970).
[11] R.H. Kraichnan, J. Fluid Mech. **77**, 753 (1976).
[12] J.A. Aronovitz and D.R. Nelson, Phys. Rev. A **30**, 1948 (1984).
[13] J.-P. Bouchaud and A. Georges, Phys. Rep. **195**, 127 (1990).
[14] M.W. Deem, Phys. Rev. E **51**, 4319 (1995).
[15] D.S. Dean, I.T. Drummond, and R.R. Horgan, Phys. Rev. E **63**, 061205 (2001).
[16] M. Dentz, H. Kinzelbach, S. Attinger, and W. Kinzelbach, Water Resour. Res. **36**, 3605 (2000).
[17] D.S. Fisher, D. Friedan, Z. Qiu, S.J. Shenker, and S.H. Shenker, Phys. Rev. A **31**, 3841 (1985).
[18] G.K. Batchelor, Austral. J. Sci. Res. **2**, 437 (1949).
[19] G.K. Batchelor, Proc. Cambridge Philos. Soc. **48**, 345 (1952).
[20] P.K. Kitanidis, J. Hydrol. **102**, 453 (1988).
[21] S. Attinger, M. Dentz, H. Kinzelbach, and W. Kinzelbach, J. Fluid Mech. **386**, 77 (1999).
[22] M. Dentz, H. Kinzelbach, S. Attinger, and W. Kinzelbach, Water Resour. Res. **36**, 3591 (2000).
[23] G. Dagan, *Flow and Transport in Porous Formations* (Springer, New York, 1989).
[24] L.W. Gelhar, *Stochastic Subsurface Hydrology* (Prentice-Hall, Englewood Cliffs, NJ, 1993).
[25] G. Dagan, Water Resour. Res. **24**, 1491 (1988).
[26] S.P. Neuman and Y.K. Zhang, Water Resour. Res. **26**, 887 (1990).
[27] Q. Zhang, Water Resour. Res. **3**, 577 (1995).
[28] T. Blum and A.J. McKane, Phys. Rev. E **52**, 4741 (1995).
[29] G. Dagan, Water Resour. Res. **10**, 2699 (1994).
[30] S. Attinger, M. Dentz, and W. Kinzelbach (unpublished).
[31] D.T. Burr and E.A. Sudicky, Water Resour. Res. **3**, 791 (1994).
[32] R.L. Naff, D.F. Haley, and E.A. Sudicky, Water Resour. Res. **34**, 679 (1998).
[33] L. Smith and F.W. Schwartz, Water Resour. Res. **17**, 351 (1980).
[34] A.F.B. Tompson and L.W. Gelhar, Water Resour. Res. **10**, 2541 (1990).
[35] A. Bellin, P. Salandin, and A. Rinaldo, Water Resour. Res. **28**, 2211 (1992).
[36] P. Salandin and V. Fiorotto, Water Resour. Res. **34**, 949 (1998).
[37] Y. Zhang and J. Lin, Stochastic Hydrol. Hydr. **12**, 117 (1998).
[38] M.B. Isichenko, Rev. Mod. Phys. **64**, 961 (1992).
[39] E.B. Tatarinova, P.A. Kalugin, and A.V. Sokol, Europhys. Lett. **14**, 773 (1991).
[40] M. Dentz, Doctoral dissertation, Ruperto-Carola-University, Heidelberg, Germany, 2000.
[41] J. Honerkamp, *Stochastic Dynamical Systems* (VCH, Weinheim, Germany, 1997).
[42] H. Risken, *The Fokker-Planck Equation*, 2nd ed. (Springer-Verlag, Heidelberg, 1996).
[43] J. Bear, *Dynamics of Fluids in Porous Media* (American Elsevier, New York, 1972).
[44] A. Weinrib and B.I. Halperin, Phys. Rev. B **26**, 1362 (1982).